ACS OMEGA

http://pubs.acs.org/journal/acsodf

Article

Pineapple-Leaf-Derived, Copper-PAN-Modified Regenerated Cellulose Sheet Used as a Hydrogen Sulfide Indicator

Surached Thongboon, Thanaphat Chukeaw, Chalida Niamnuy, Supacharee Roddecha, Paweena Prapainainar, Metta Chareonpanich, Passakorn Kingwascharapong, Kajornsak Faungnawakij, Günther Rupprechter, and Anusorn Seubsai*

Cite This: *ACS Omega* 2023, 8, 17134−17142

Read Online

ACCESS | Metrics & More | Article Recommendations | Supporting Information

ABSTRACT: Regenerated cellulose (RC) produced from waste pineapple leaves was used to develop a colorimetric sensor as a Cu-PAN sheet (RCS). Microcrystalline cellulose derived from dried pineapple leaves was combined with Cu-PAN, dissolved in NaOH and urea, and made into an RC sheet using Na_2SO_4 as a coagulant. The RCS was used as an H_2S indicator at various H_2S concentrations (0−50 ppm) and temperatures (5−25 °C). The RCS color changed from purple to New York pink when exposed to H_2S. A colorimeter method was used to develop prediction curves with values of $R^2 > 0.95$ for H_2S concentrations at 5−25 °C. The physicochemical properties of fresh and spent RCS were characterized using various techniques (Fourier transform infrared spectroscopy, X-ray diffraction, scanning electron microscopy/energy-dispersive X-ray spectroscopy, and thermogravimetric analysis). In addition, when stored at 5 and 25 °C for 90 days, the RCS had outstanding stability. The developed RCS could be applied to food packaging as an intelligent indicator of meat spoilage.

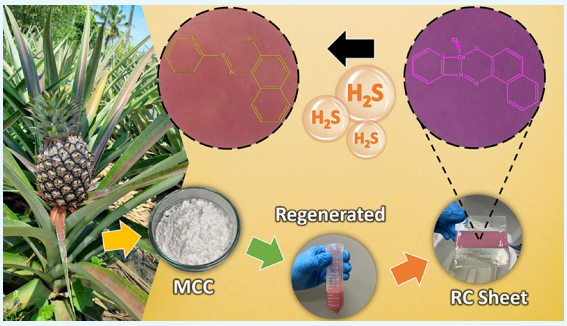

1. INTRODUCTION

Currently, Thailand is one of the world's top cultivators and exporters of agricultural products.[1] As a result, there is a lot of agricultural waste, such as rice straw, bagasse, kapok, cotton scraps, banana trees, pineapple leaves, palm residue, sawdust, and corn cobs. If these agricultural wastes are not converted into fuel or animal feed, they are disposed of as waste, which can be costly and potentially environmentally undesirable. For example, pineapple leaves are primarily abandoned in landfill after harvest. In Thailand, there is an estimated 56 tons of pineapple leaves produced per hectare, which amounted to approximately 4 million tons of pineapple leaves produced in 2020.[2] Usually, according to the variety of pineapple and the region where it was harvested, dried pineapple leaves consist of α-cellulose (75−87%), hemicellulose (12−20%), lignin (3−9%), and other substances (such as wax, oil, pectin, tannin, and water).[3]

Cellulose is an abundant biopolymer and a renewable natural material used in numerous applications, including degradable plastic, food, and drug delivery.[4] An exciting application is its dissolution in deep eutectic solvents (DESs) and ionic liquids to obtain regenerated cellulose (RC).[5−8] Both DESs and ionic liquids are regarded as ecologically friendly solvents for cellulose because of their low toxicity and volatility.[6,8] The DESs can be created by combining a hydrogen bond acceptor (e.g., choline chloride, proline betaine, and urea) and a hydrogen bond donor (e.g., glycerol, ethylene glycol, glucose, xylose, fructose, and urea).[6] Ionic liquids are organic salts that appear as liquids at comparatively low temperatures (below 100 °C).[8] Ionic liquids like imidazolium-based ionic liquids,[9,10] 1-butyl-3-methylimidazolium chloride,[11] *N*-methylmorpholine-*N*-oxide,[12] and tetrabutylphosphonium hydroxide[13] can be used to dissolve cellulose. One environmentally friendly approach is to use NaOH and urea as the solvent, allowing the rapid disruption of inter-/intramolecular hydrogen bonds at low temperatures.[14] Then, a coagulant (such as H_2SO_4,[15] $NaSO_4$,[16] or water[17]) is used to precipitate the dissolved cellulose into the RC film. Notably, the coagulation conditions, nature, and mechanism are critical in controlling the structural and morphological properties of the RC film.[14,18] The degradable RC film is often used as an active or intelligent packaging material because it possesses a three-dimensional porous structure that allows the merging of functional fillers.[19] Different modified cellulose films have been made for various applications in the past few years. Zhao et al. prepared a biodegradable film from durian-rind cellulose with a good appearance and excellent transparency for packaging

Received: March 3, 2023
Accepted: April 24, 2023
Published: May 2, 2023

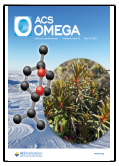

applications. The film completely disintegrated in 4 weeks.[20] Gu et al. demonstrated an antibacterial cellulose film modified with silver nanoparticles (AgNPs) as food packaging to extend the shelf life of food.[21] Ding et al. created a pH sensor prepared from polyvinyl alcohol and dye-modified cellulose, which acted as a superior shrimp spoilage detector and had excellent leakage resistance properties.[22]

Spoilage of some foods (e.g., meat, poultry, and fish) causes emissions of hydrogen sulfide (H_2S) gas or rotten egg gas, which is colorless, flammable, poisonous, and corrosive.[23] The decomposition of microorganisms in food, food waste, and wastewater without oxygen usually generates this gas. H_2S gas can cause respiratory symptoms even if the gas concentration is small (10 ppm).[24] Hence, detecting and controlling H_2S gas in nonlethal quantities is crucial for human and industrial health. Industries that could benefit from having an H_2S detection system include refining, mining, tanning, pulp and paper processing, rayon manufacturing, and food packaging.[25−27] Focusing on food packaging, an intelligent indicator is of great interest for detecting food spoilage of meat inside the packaging.

In certain types of food packaging—such as modified atmosphere packaging,[28] in which a gas atmosphere usually consisting of an inert gas (e.g., N_2) along with an antimicrobial active gas (e.g., CO_2) is added to a packaged food product to increase its shelf life—H_2S can form due to microbial growth.[29] Several techniques can be used to detect H_2S in food containers.[27,30−32] Colorimetric test strips, for example, are paper strips placed inside the food package that changes color in the presence of H_2S.[27] Alternatively, electronic sensors can identify H_2S and generate a digital readout of the H_2S concentration. These sensors are more precise than colorimetric test strips but also more expensive.[33] Similarly, gas chromatography, a lab-based technique, entails removing the gas from the food package and analyzing it with specialized tools. Gas chromatography is extremely accurate but time-consuming and expensive and requires specific knowledge and tools.[32] Depending on the packaging material, the food product, and the packaging procedure, a particular H_2S detection technique is used. It is crucial to choose a suitable detection technique to ensure the safety and quality of the food product.

In the colorimetric methods, metal complexes are used to detect H_2S gas. For example, Pb(II) acetate-based materials are widely used to detect H_2S gas, which can be noticed by the color change from white to dark brown when H_2S gas is detected. However, the disadvantage is that Pb is highly toxic and unstable.[34] AgNPs have also been studied extensively for use in H_2S detection. AgNPs have been modified with polyethylenimine,[35] gellan gum,[36] and nylon.[37] The color of the AgNP-based materials will change from colorless to light yellow when in contact with H_2S. Nevertheless, AgNPs are relatively expensive. Complex compounds can also be used as color indicators for H_2S detection. For example, *N*,*N*-dimethyl-*p*-phenylenediamine has been frequently mentioned as a reliable indicator in many research projects.[38−41] After exposure to H_2S, this complex structure is transformed into methylene blue using $FeCl_3$ as a catalyst; the color changes from colorless to blue.[38] However, its toxicity is of concern; thus, its application in food packaging has not been suitable.[42] Another means of H_2S detection that is becoming more popular is the use of copper(II) pyridine diazinonaphthol (Cu-PAN). This is interesting because when exposed to H_2S gas, its color rapidly changes from purple to yellow and this change is visible to the naked eye.[39,42,43] Most importantly, it is nontoxic to humans and low cost.[38−41,43]

The current work involved the creation of a colorimetric sensor as an RC sheet from Cu-PAN modified with RC derived from pineapple leaves leftover from agriculture. The pineapple leaves were extracted using NaOH solution, bleached with $NaClO_2$ + acetic acid, and hydrolyzed with HCl solution to obtain microcrystalline cellulose (MCC). After that, the MCC was dissolved using NaOH + urea, mixed with Cu-PAN, and finally regenerated as an RC sheet using Na_2SO_4 as a coagulant. The RC sheet modified with Cu-PAN (RCS) was used as an H_2S indicator at different H_2S concentrations and temperatures. Prediction curves for the H_2S concentration at different temperatures were developed using a colorimeter method with the RCS after being exposed to H_2S gas for 30 min. In addition, the basic physicochemical properties and the stability of the RCS were investigated.

2. RESULTS AND DISCUSSION

2.1. Physical and Chemical Properties of MCC and RCS. *2.1.1. Naked-Eye Inspection of the Samples.* The chopped dried pineapple leaves, extracted cellulose fiber, MCC, and fresh RCS (RCS-F) are illustrated in Figure 1. As

Figure 1. (a) Dried pineapple leaves, (b) extracted cellulose fiber, (c) MCC, and (d) RCS-F.

can be seen, after the chopped dried pineapple leaves (Figure 1a) were extracted using an NaOH solution at 90 °C for 2 h to eliminate non-cellulose compounds, such as lignins and waxes, followed by bleaching at pH = 5 at 70 °C for 30 min, white fibrous cellulose was obtained (Figure 1b). Next, the fibrous cellulose was hydrolyzed using an HCl solution at 70 °C for 30 min, washed with DI water, dried in a freeze dryer at 0.5 torr and −43 °C for 16 h, and then ground to a fine white powder, namely, MCC (Figure 1c). Afterward, the MCC was well mixed with Cu-PAN, cast on a glass plate, and immersed in a coagulant (an aqueous solution of Na_2SO_4) for 15 min to generate a fresh thin sheet (1.0 mm thickness) of RC, namely, RCS-F (Figure 1d).

2.1.2. Sample Analysis with X-ray Diffraction. The X-ray diffraction (XRD) patterns of the MCC, RCS-F, and RCS-S are displayed in Figure 2. The XRD peaks at 2θ = 14.5, 16.5, and 22.5° for MCC corresponded to the crystallinity structural pattern of cellulose I.[44] For RCS-F and RCS-S, the XRD peaks appearing at 2θ = 12.1 and 19.8° indicated the crystalline structure of cellulose II. In addition, peaks at 2θ = 14.5 and 16.5° were also observed, suggesting that the cellulose I of MCC transformed to cellulose II after being modified with Cu-

https://doi.org/10.1021/acsomega.3c01449
ACS Omega 2023, 8, 17134−17142

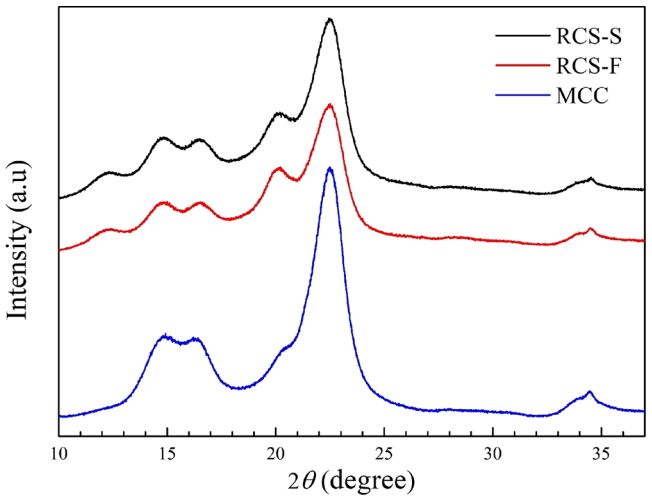

Figure 2. XRD patterns of MCC, RCS-F, and RCS-S.

PAN, but not completely. Note that the analysis of the samples with the Fourier transform infrared spectra was also performed (see Figure S1). The FTIR spectra of these three samples were almost identical probably due to the relatively low concentration of Cu species in the RCS-F and RCS-S samples.

2.1.3. Sample Analysis with Scanning Electron Microscopy/Energy-Dispersive X-ray Spectroscopy. The surface morphologies of MCC, RCS-F, and RCS-S were characterized using scanning electron microscopy/energy-dispersive X-ray spectroscopy (SEM/EDS), as shown in Figure 3. The SEM image of MCC (Figure 3b) indicated rod-shaped fibers with an average length of approximately 25 μm. After doping with Cu-PAN, the SEM image of RCS-F (Figure 3d) had rough surfaces resulting from the uniform dispersion of undissolved cellulose fibers. This also suggested that a portion of MCC was dissolved. After the residue cellulose fibers mixed with Cu-PAN were immersed into the coagulant, the RCS-F was formed. The inserted EDS-mapping images in Figure 3d of RCS-F demonstrate the distribution of C and Cu throughout the cellulose sheet, confirming the successful modification of MCC by adding Cu-PAN. After being used, the surface morphology of RCS-S (Figure 3f) was not much different compared to the fresh one. The inserted EDS-mapping images of RCS-S show the presence of C, Cu, and S, confirming that the H_2S adsorption into the RCS had occurred.

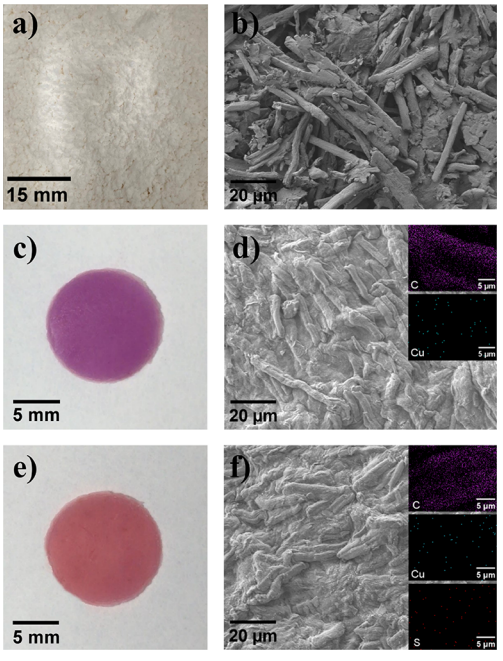

Figure 3. Naked-eye images and SEM images, respectively: (a, b) MCC, (c, d) RCS-F with EDS images of C and Cu, and (e, f) RCS-S with EDS images of C, Cu, and S.

2.1.4. Sample Analysis with Thermogravimetric Analysis. The degradation and thermal stability of the samples were performed using thermogravimetric analysis (TGA) in the temperature range 30−800 °C, as shown in Figure 4. In Figure 4a, the TGA curves of all samples could be separated into two stages. The first stage for a temperature from 30 to 150 °C showed weight loss corresponding to the evaporation of water absorbed to the cellulose structure,[45] while the second stage was related to decarboxylation and depolymerization of the cellulose.[46] In addition, the differential thermal analysis (DTA) (Figure 4b) of the RC showed that adding Cu-PAN had a maximum decomposed temperature higher than the original cellulose (MCC) probably because MCC has a higher crystalline value compared to the RC.[47] Accordingly, modifying the cellulose sheet by adding Cu-PAN improved the temperature stability of the RC.

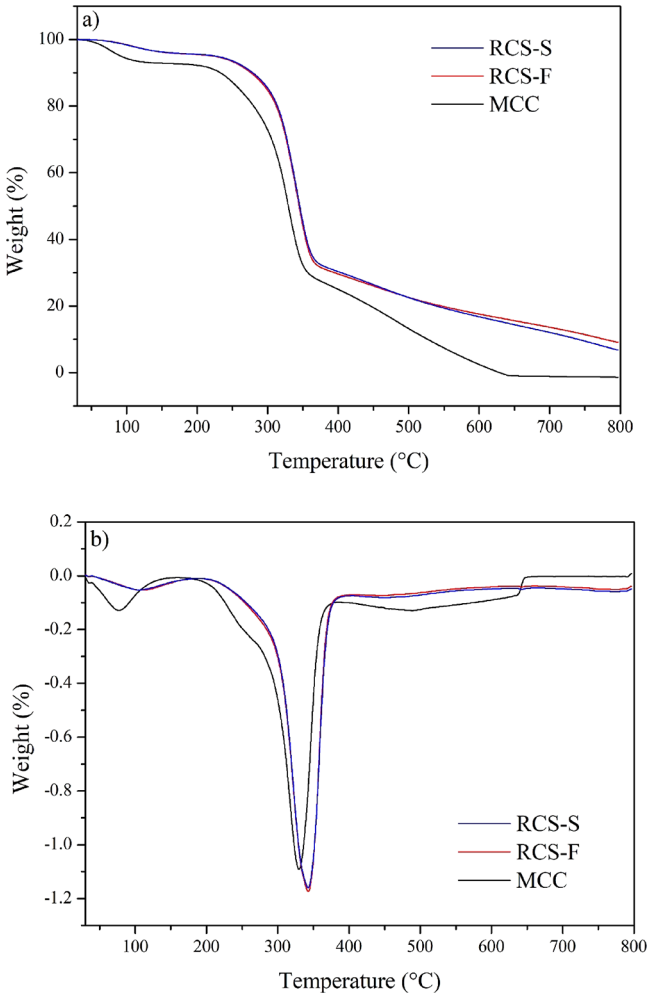

Figure 4. (a) TGA and (b) DTA curves of MCC, RCS-F, and RCS-S.

https://doi.org/10.1021/acsomega.3c01449
ACS Omega 2023, 8, 17134−17142

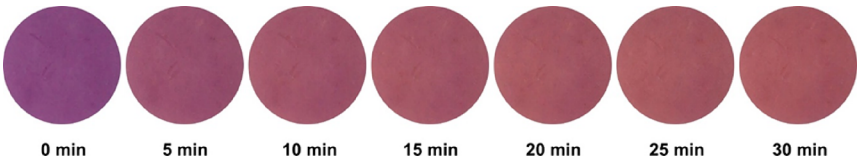

Figure 5. Color change of the Cu-PAN cellulose sensor during 30 min exposure to H_2S at 50 ppm.

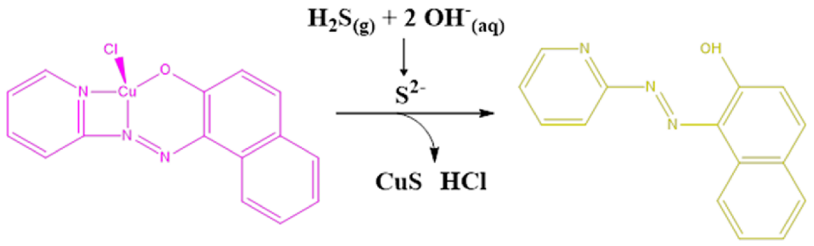

Figure 6. Reaction mechanism of Cu-PAN and H_2S. Reprinted (Adapted or Reprinted in part) with permission from Carpenter, T. S.; Rosolina, S. M.; Xue, Z. L., Quantitative, colorimetric paper probe for hydrogen sulfide gas. *Sens. Actuators B Chem.* **2017**, *253*, 846−851. Copyright 2017 Elsevier B.V.

Table 1. Colorimetric Data of the RCS when Exposed to H_2S at Different H_2S Concentrations and Temperatures

H_2S (ppm)	Temperature (°C)				
	5	10	15	20	25
0			L* =45.77 a* = 34.05 b* = -19.46		
10	L* = 39.43 a* = 33.72 b* = -9.73	L* = 45.62 a* = 34.82 b* = -9.83	L* =41.63 a* = 34.68 b* = -7.21	L* = 45.41 a* = 35.39 b* = -6.28	L* = 45.57 a* = 30.22 b* = -3.75
20	L* = 40.97 a* = 35.07 b* = -7.39	L* = 45.16 a* = 33.53 b* = -7.08	L* =43.86 a* = 32.46 b* = -2.21	L* = 41.46 a* = 33.59 b* = -2.12	L* = 43.93 a* = 35.10 b* = -0.87
40	L* = 39.98 a* = 34.34 b* = 1.43	L* = 39.54 a* = 33.19 b* = 2.49	L* = 46.18 a* = 34.44 b* = 4.93	L* = 45.95 a* = 34.55 b* = 9.31	L* = 50.79 a* = 33.50 b* = 10.43
50	L* = 52.12 a* = 34.16 b* = 4.29	L* = 47.10 a* = 38.09 b* = 4.91	L* =46.79 a* = 33.24 b* =10.70	L* = 50.64 a* = 32.35 b* = 10.12	L* = 51.63 a* = 31.86 b* =12.39

2.2. H_2S Adsorption Performance of the RCS. Following its successful preparation, the RCS-F was used to study adsorption with H_2S gas. Initially, the concentration of H_2S in N_2 was 50 ppm and the adsorption time was 30 min. The reactivity of the Cu-PAN cellulose with H_2S was monitored every 5 min, as shown in Figure 5. As observed, the Cu-PAN cellulose film underwent a color change from purple to New York pink, which was visible to the naked eye.

The color change was expressed in terms of the reaction mechanism, as shown in Figure 6. When the Cu-PAN complex was exposed to H_2S, the H_2S was dissolved by the water and released S^{2-}, which caught Cu^{2+} in the Cu-PAN complex to form CuS and H-PAN. The colors of pure CuS and H-PAN are black[48] and yellow,[43] respectively. Thus, the overall color of the Cu-PAN cellulose film after exposure to H_2S was New York pink. Analytical techniques that can be used to detect color change include UV−vis, HPLC-UV, and colorimetric methods.[39]

The Cu-PAN cellulose film was measured for its efficiency to determine the presence of H_2S using a colorimeter, as

https://doi.org/10.1021/acsomega.3c01449
ACS Omega 2023, 8, 17134−17142

described in Section 4.5. Table 1 shows the color change of the Cu-PAN cellulose films at H_2S concentrations of 10, 20, and 50 ppm in the temperature range from 5 to 25 °C. This temperature range was chosen because it is the usual storage temperature for fresh food in supermarkets. It was found that for every temperature, increasing the H_2S concentration gradually increased the b^* value of the Cu-PAN cellulose film and considerably changed when compared to the other color values.

The plots between the b^* value of the RCS after it had been exposed to H_2S at different initial concentrations of H_2S for 30 min at the same temperature *versus* the initial concentration of H_2S are shown in Figure 7. The slopes of the curves of the

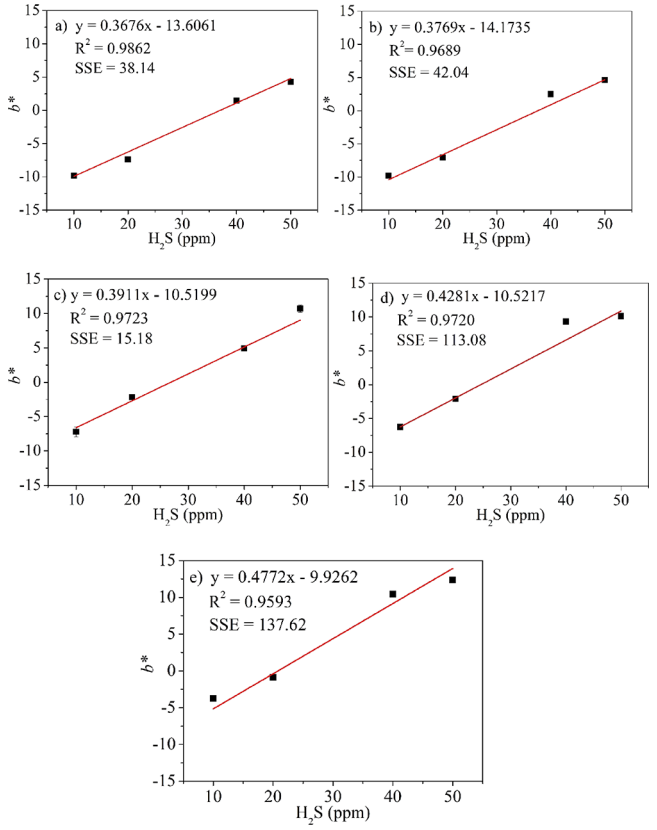

Figure 7. Calibration curves indicating data correlation between b^* values and concentrations of H_2S gas at (a) 5 °C, (b) 10 °C, (c) 15 °C, (d) 20 °C, and (e) 25 °C.

RCS at 5, 10, 15, 20, and 25 °C were 0.368 (coefficient of determination or R^2 = 0.986), 0.377 (R^2 = 0.969), 0.391 (R^2 = 0.972), 0.428 (R^2 = 0.972), and 0.477 (R^2 = 0.959), respectively. Furthermore, to determine the error difference between the observed and predicted values, the sum square of error (SSE) of each curve was calculated, as presented in each plot (see Figure 7). The formula for SSE has been reported elsewhere.[3] Clearly, all the R^2 values were greater than 0.95, and all the SSE values were relatively low to medium (15−138), indicating that the linear regression models were good fits with the experimental data. It should be noted that, as in other reports,[43,49] the fitted straight line for each temperature does not include the origin (0 ppm of H_2S). If it had, an excellent straight line could not be obtained. This implies that the behavior of the chemical reaction and/or the color change is unpredictable when the concentration of H_2S is far below the experimental range. Furthermore, the limit of detection (LOD) value for H_2S at each temperature was determined using eq 1:[50]

$$\text{Limit of detection} = \frac{3.3\text{SD}}{m} \tag{1}$$

where SD is the standard deviation of the intercept ($\text{SD} = \text{SE}\sqrt{N}$), SE is the standard error of intercept from regression, N is the number of tests, and m is the slope of the calibration curve. It was found that the values of LOD at 5, 10, 15, 20, and 25 °C were 17.61, 15.69, 24.23, 19.13, and 22.98 ppm, respectively. Notably, the slopes for the temperatures ranging from 20 to 25 °C were steeper than the others, suggesting that this temperature range was the most sensitive to H_2S detection. The experimental results were also verified by testing the RCS-F with H_2S at 35 ppm and 15 °C. It was found that the experiment yielded a b^* value of 3.17, while the calculated value using the linear equation at 15 °C gave a b^* value of 3.24. The difference in the values resulted in an error of 2.25%, one acceptable for practical uses.

2.3. Stability of the RCS. The stability of RCS-F was investigated by storing it at 5 and 25 °C for 90 days. The colorimetric measurements of the material were carried out on the 1st, 5th, 15th, and 90th days. Each RCS-F sample was soaked, placed in a Petri dish with a glass cover, and kept in a refrigerator (5 °C) or a temperature control room (25 °C). The samples in both storage temperatures were stored in the dark except when being inspected. Moreover, the samples were kept soaked to prevent the RCS-F from drying and cracking. Then, after 90 days of storage, each RCS-F sample was subjected to H_2S detection at 500 ppm for 30 min at the sample storage temperature. As observed, the samples for both storage temperatures remained in excellent shape and color throughout the 90 days of storage (Figure 8a,c). After the H_2S adsorption, the color change was as expected (Figure 8b,d). However, in each case, the b^* value was lower than what was found for the same conditions, as presented previously in Table 1. The reduction efficiency of H_2S detection was calculated using eq 2:

$$\%\text{Reduction efficiency of } H_2S \text{ detection} = \frac{\Delta b^*_{\text{fresh}} - \Delta b^*_{\text{storage}}}{\Delta b^*_{\text{fresh}}} \times 100 \tag{2}$$

where $\Delta b^*_{\text{fresh}} = (b^*_{\text{RCS-F}} - b^*_{\text{RCS-S}})_{\text{fresh}}$ and $\Delta b^*_{\text{storage}} = (b^*_{\text{RCS-F}} - b^*_{\text{RCS-S}})_{\text{day 90}}$. The levels of reduction efficiency of H_2S detection of the sample stored at 5 and 25 °C were 76 and 43%, respectively, indicating that RCS-F was still outstanding with regard to sheet form and color after 90 days of storage. Nonetheless, the H_2S detection effectiveness had decreased, which may have been caused by Cu-PAN decomposition due to the exposure to moisture for an excessive time.

2.4. H_2S Sensing Performance of the RCS Compared to Other Relevant Materials. The H_2S detection performance of the RCS-F samples was compared with other reports, as shown in Table 2. Note that the publications listed in Table 2 are materials that exhibit a color change when inspected with the naked eye. The lowest H_2S detection in the current work was 22.98 ppm at 25 °C. Some materials can detect H_2S below 1 ppm, such as Cu(II)-azo complex-modified hydrogel[49] and Cu-PAN layers printed on coated paper.[43] Notably, some of

https://doi.org/10.1021/acsomega.3c01449
ACS Omega 2023, 8, 17134−17142

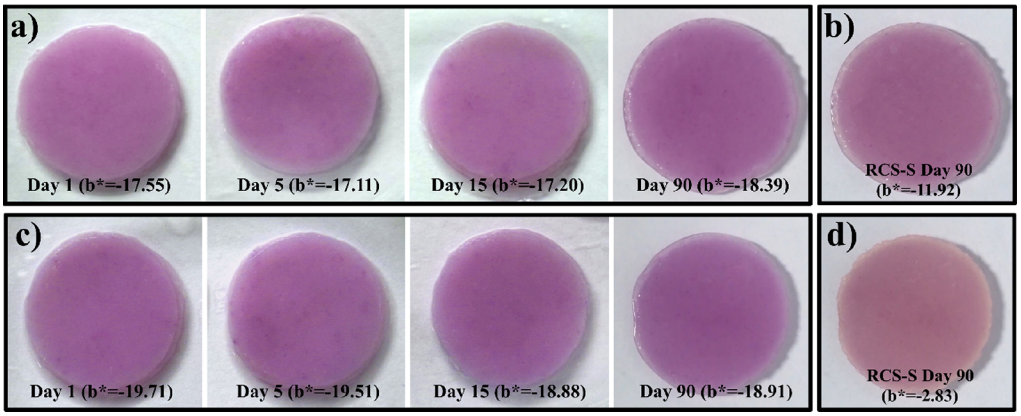

Figure 8. Naked-eye images of RCS-F samples stored in a closed container in (a) a refrigerator at 5 °C and (c) a temperature control room at 25 °C, where (b) and (d) show naked-eye images of RCS-S right after RCS-F (at day 90) was exposed to H_2S at an initial H_2S concentration of 50 ppm for 30 min at 5 and 25 °C, respectively.

Table 2. H_2S Sensing Performance Compared to Other Cu-Based Materials[a]

material	limit of detection (ppm)	conditions	reference no.
Cu-PAN-modified RC sheet (RCS-F)	22.98	25 °C, 60% humidity, 30 min	this work
copper(II)-azo complex-modified hydrogel	0.04334	room temperature, 10 min	49
paper probe modified with Cu-PAN	0.016	room temperature, 10% humidity, 5 min	43
Cu-PAN layers printed on coated paper	8	room temperature, 40% humidity, 20 min	42
printed paper (ethyl cellulose mixed with Cu-PAN)	4	room temperature, 40% humidity, 15 min	39
microplate cover coated with Nafion polymer doped with Ag^+	212	37 °C, 40 min	51
paper strip soaked with DNPS (dansyl-naphthalimide conjugated sulfonamide)	2	room temperature, 30 min, vacuum	52
paper impregnated with $FeCl_3$ and *N*,*N*-dimethyl-*p*-phenylenediamine	1.11	30 min	38
solution of Au nanoparticles	0.5	room temperature, 15 min	53
solution of thiolated azido derivates and active esters functionalized Au nanoparticles	5		54

[a]The publications presented here are limited to those that reported color change in the sensing material from naked-eye inspection.

these publications reported H_2S gas generation from an in-house H_2S-generating process by combining Na_2S and HCl solutions in a vessel,[43] which could have been due to strict regulations in different countries regarding the purchase of H_2S gas. This would be an excellent optional approach to producing H_2S for academic purposes. Although the RCS-F had slightly lower H_2S sensitivity than the other materials, our developed H_2S sensor, which was made from agricultural waste (pineapple leaves), was relatively inexpensive, durable, and practical, suggesting that it has great potential for use in a variety of applications, particularly for food packaging to detect any spoilage of meat inside the container.

3. CONCLUSIONS

The RCS-F was successfully prepared from pineapple leaves through extraction, bleaching, hydrolysis, dissolution, and precipitation with Cu-PAN. The RCS-F was cut into a coin shape (1.2 cm in diameter and 0.1 cm in thickness) and used for H_2S adsorption at 5−25 °C. The fresh RCS was purple and changed to New York pink after being exposed to H_2S, which was visible to the naked eye. A higher concentration of H_2S and a higher temperature resulted in a more visible change in the RCS color. The b^* values acquired from the colorimetric measurements at various H_2S concentrations were used to forecast the H_2S concentration in the temperature range of 5 to 25 °C. The results indicated that a straight line with an R^2 > 0.95 with a low-to-medium SSE value was obtained for every temperature, indicating that the color change could be applied to calculate the H_2S concentration. In addition, when stored in wet conditions, the condition and functioning of the RCS remained steady for over 90 days, although the effectiveness of the H_2S measurement was reduced. This work demonstrated that pineapple leaves could be used to create an RC sheet that could then be altered using Cu-PAN to create an H_2S indicator, which could be applied in meat packaging to improve safety and health management.

4. MATERIALS AND METHODS

4.1. Extraction of Pineapple Leaf Fibers. The alkaline treatment was performed according to the methodology explained by Chanka et al. (2021). First, pineapple leaves (PALs) were chopped into small sheet pieces and dried at 65 °C in an atmospheric hot-air oven for 48 h. Then, the PALs were treated with a 10% w/w solution of NaOH at 90 °C to eliminate non-cellulose components (lignin and wax) under stirring for 2 h. Afterward, the dark brown solution was filtered through stainless steel sieves and neutralized with hot water several times. Next, the residue was bleached using 1% (w/v) $NaClO_2$ and acetic acid to adjust to pH = 5 at 70 °C for 30 min. Finally, the bleached PAL fibers were washed with distilled water until a neutral pH was reached and then dried at 65 °C in a hot-air oven for 24 h.

https://doi.org/10.1021/acsomega.3c01449
ACS Omega 2023, 8, 17134−17142

4.2. Preparation of MCC. To prepare the MCC from the extracted PAL fibers, initially, 10 g of PAL fibers was depolymerized using 500 mL of 3.5 M HCl under stirring at 70 °C for 30 min. After hydrolyzing, 4000 mL of distilled water was added to the suspension. Then, the mixture was divided into small portions (50 mL per container) and each portion was centrifuged at 8000 rpm for 5 min to separate the clear solution from the white solid. Then, 40 mL of distilled water was added to the white part of each portion and the centrifugal process was repeated. This process was repeated until a neutral pH was recorded. The white paste was dehydrated in a freeze drier (Harvest Right; USA) at 0.5 torr and −43 °C for 16 h. Finally, the obtained white sample (MCC) was ground into a fine powder.

4.3. Preparation of Cu-PAN. The Cu-PAN was synthesized as reported by Carpenter et al. (2017).[43] A solution of 0.085 g of copper(II) chloride dihydrate (Qrec; New Zealand) in 3 mL of deionized (DI) water was added to 0.124 g of 1-(2-pyridylazo)-2-naphthol (Thermo Scientific; India) in 75 mL of ethanol (Qrec; New Zealand). Then, the mixture was stirred at room temperature for 12 h. The dark red sediment was filtered and washed with ethanol (3 mL) three times and then dried at room temperature.

4.4. Preparation of RC Sheet-Doped Cu-PAN. A solution (7 mL) of NaOH (Fisher Scientific; UK) mixed with urea (KemAus; Australia) at a ratio of NaOH-to-urea-to-DI water of 7.5:11.0:81.5 by weight was first precooled at −12 °C in a refrigerator, as described by Zhang et al. (2005).[18] After that, 1 g of MCC and 0.0025 g of Cu-PAN were added to the solution rapidly under vigorous stirring for 10 min at room temperature. The obtained viscous solution was centrifuged to degas and then cast 1 mm thick on a glass plate. Next, the translucent, dissolved cellulose was soaked in aqueous Na_2SO_4 5 wt % as a coagulant for 15 min to generate a thin sheet. Finally, it was rinsed with DI water to obtain a thin wet sheet of cellulose doped with Cu-PAN, namely, RCS-F.

4.5. H_2S Gas Measurements. At atmospheric pressure, the RCS-F was tested with H_2S gas in a sealed, temperature-controlled chamber. The chamber system had been developed in the laboratory, as shown in Figure 9. Before testing, the soaked RCS-F in DI water was removed and free water was allowed to drain to produce a sheet moisture content of approximately 0.75% (wet basis). The sheet was placed into the chamber, and then the controller was adjusted to the desired temperature to keep the humidity within the range of 50−60%. Next, a known amount of H_2S gas in a syringe was injected into the box along with the process time and videoed for 30 min to record the color change in the cellulose film using a colorimeter (model LS171, China) obtained from Shenzhen Linshang Technology and the Commission Internationale de l'Eclairage "Lab" (CIE $L^*a^*b^*$) system was applied to determine constituent color values, where L^* represents the brightness from white ($+L^*$) to black ($-L^*$), a^* represents the color from green ($-a^*$) to red ($+a^*$), and b^* represents the color from blue ($-b^*$) to yellow ($+b^*$).

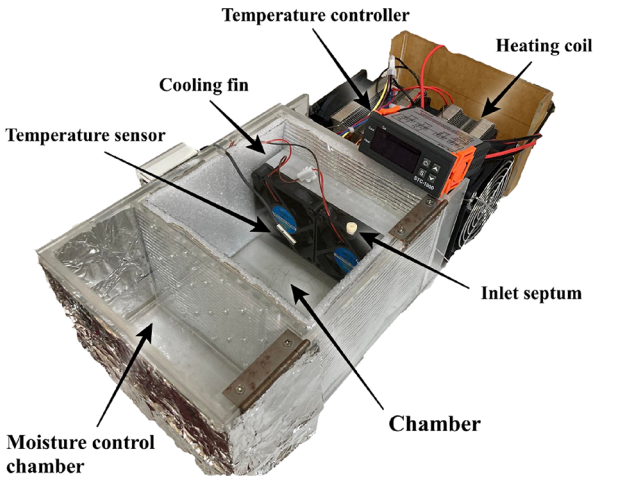

Figure 9. Components of the sealed, temperature-controlled chamber used for H_2S measurements.

4.6. Material Characterization. *4.6.1. Thermogravimetric Analysis.* TGA of all samples was measured using a thermogravimetric instrument (model TGA/SDTA 851e; Mettler Toledo; USA). The thermal analysis method was performed in an air environment at a heating rate of 10 °C min^{-1} from 30 to 800 °C.

4.6.2. Scanning Electron Microscopy and Energy-Dispersive X-ray Spectroscopy. The structure and morphology of all cellulose samples were analyzed using a scanning electron microscope (FE-SEM; JSM7600F; JEOL; Japan) at an operating voltage of 2.0 kV. An energy-dispersive X-ray spectrometer (EDS) was used to undertake elemental analysis based on qualitative and quantitative mapping of all specimens.

4.6.3. X-ray Diffraction. The crystallinity structure of each sample was determined using an X-ray diffractometer (XRD; SmartLab SE; Rigaku; Japan). The XRD patterns with Cu K_α radiation (wavelength = 0.154) at 40 kV and 100 mA were collected in the range 2θ from 10 to 40° at a scan step of 0.02° min^{-1}.

■ ASSOCIATED CONTENT

Supporting Information

The Supporting Information is available free of charge at https://pubs.acs.org/doi/10.1021/acsomega.3c01449.

Information and figure of FTIR spectra (PDF)

■ AUTHOR INFORMATION

Corresponding Author

Anusorn Seubsai − *Department of Chemical Engineering, Faculty of Engineering and Center of Excellence on Petrochemical and Materials Technology, Kasetsart University, Bangkok 10900, Thailand;* orcid.org/0000-0001-8336-6590; Email: fengasn@ku.ac.th

Authors

Surached Thongboon − *Department of Chemical Engineering, Faculty of Engineering, Kasetsart University, Bangkok 10900, Thailand*

Thanaphat Chukeaw − *Department of Chemical Engineering, Faculty of Engineering, Kasetsart University, Bangkok 10900, Thailand*

Chalida Niamnuy − *Department of Chemical Engineering, Faculty of Engineering, Kasetsart University, Bangkok 10900, Thailand;* orcid.org/0000-0003-2932-2022

Supacharee Roddecha − *Department of Chemical Engineering, Faculty of Engineering, Kasetsart University, Bangkok 10900, Thailand;* orcid.org/0000-0001-7675-9804

https://doi.org/10.1021/acsomega.3c01449
ACS Omega 2023, 8, 17134−17142

Paweena Prapainainar − *Department of Chemical Engineering, Faculty of Engineering, Kasetsart University, Bangkok 10900, Thailand*

Metta Chareonpanich − *Department of Chemical Engineering, Faculty of Engineering and Center of Excellence on Petrochemical and Materials Technology, Kasetsart University, Bangkok 10900, Thailand;* orcid.org/0000-0002-4333-337X

Passakorn Kingwascharapong − *Department of Fishery Products, Faculty of Fisheries, Kasetsart University, Bangkok 10900, Thailand*

Kajornsak Faungnawakij − *National Nanotechnology Center (NANOTEC), National Science and Technology Development Agency (NSTDA), Pathum Thani 12120, Thailand;* orcid.org/0000-0002-4724-0613

Günther Rupprechter − *Institute of Materials Chemistry, Technische Universität Wien, Vienna 1060, Austria;* orcid.org/0000-0002-8040-1677

Complete contact information is available at: https://pubs.acs.org/10.1021/acsomega.3c01449

Notes

The authors declare no competing financial interest.

■ ACKNOWLEDGMENTS

This work was financially supported by the Fundamental Fund, Thailand (FF(KU)12.66); the Kasetsart University Research and Development Institute (KURDI), Bangkok, Thailand; the Office of the Ministry of Higher Education, Science, Research and Innovation, Thailand; the Thailand Science Research and Innovation through the Kasetsart University Reinventing University Program 2021; and the National Research Council of Thailand through the Research Team Promotion Grant/Senior Research Scholar (grant no. N42A640324).

■ REFERENCES

(1) Food and Agriculture Organization of the United Nations (FAO). *World Food and Agriculture - Statistical Yearbook* 2020, Rome, Italy.

(2) Office of Agricultural Economics. *Agricultural Statistics of Thailand* 2020. Bangkok, Thailand.

(3) Daochalermwong, A.; Chanka, N.; Songsrirote, K.; Dittanet, P.; Niamnuy, C.; Seubsai, A. Removal of heavy metal ions using modified celluloses prepared from pineapple leaf fiber. *ACS Omega* **2020**, *5*, 5285−5296.

(4) Aziz, T.; Ullah, A.; Ali, A.; Shabeer, M.; Shah, M. N.; Haq, F.; Iqbal, M.; Ullah, R.; Khan, F. U. Manufactures of bio-degradable and bio-based polymers for bio-materials in the pharmaceutical field. *J. Appl. Polym. Sci.* **2022**, *139*, No. e52624.

(5) Zainul Armir, N. A.; Zulkifli, A.; Gunaseelan, S.; Palanivelu, S. D.; Salleh, K. M.; Che Othman, M. H.; Zakaria, S. Regenerated cellulose products for agricultural and their potential: A review. *Polymer* **2021**, *13*, 3586.

(6) Bjelić, A.; Hočevar, B.; Grilc, M.; Novak, U.; Likozar, B. A review of sustainable lignocellulose biorefining applying (natural) deep eutectic solvents (DESs) for separations, catalysis and enzymatic biotransformation processes. *Rev. Chem. Eng.* **2022**, *38*, 243−272.

(7) Mamilla, J. L. K.; Novak, U.; Grilc, M.; Likozar, B. Natural deep eutectic solvents (DES) for fractionation of waste lignocellulosic biomass and its cascade conversion to value-added bio-based chemicals. *Biomass Bioenergy* **2019**, *120*, 417−425.

(8) Zhu, S.; Wu, Y.; Chen, Q.; Yu, Z.; Wang, C.; Jin, S.; Ding, Y.; Wu, G. Dissolution of cellulose with ionic liquids and its application: a mini-review. *Green Chem.* **2006**, *8*, 325−327.

(9) Grilc, M.; Likozar, B.; Levec, J. Kinetic model of homogeneous lignocellulosic biomass solvolysis in glycerol and imidazolium-based ionic liquids with subsequent heterogeneous hydrodeoxygenation over $NiMo/Al_2O_3$ catalyst. *Catal. Today* **2015**, *256*, 302−314.

(10) Zhang, J.; Wu, J.; Yu, J.; Zhang, X.; He, J.; Zhang, J. Application of ionic liquids for dissolving cellulose and fabricating cellulose-based materials: State of the art and future trends. *Mater. Chem. Front.* **2017**, *1*, 1273−1290.

(11) Kotov, N.; Raus, V.; Urbanová, M.; Zhigunov, A.; Dybal, J.; Brus, J. Impact of cellulose dissolution on 1-butyl-3-methylimidazolium chloride crystallization studied by Raman spectroscopy, wide-angle x-ray scattering, and solid-state NMR. *Cryst. Growth Des.* **2020**, *20*, 1706−1715.

(12) Perepelkin, K. E. Lyocell fibres based on direct dissolution of cellulose in N-methylmorpholine N-oxide: Development and prospects. *Fibre Chem.* **2007**, *39*, 163−172.

(13) Abe, M.; Fukaya, Y.; Ohno, H. Fast and facile dissolution of cellulose with tetrabutylphosphonium hydroxide containing 40 wt% water. *Chem. Commun.* **2012**, *48*, 1808−1810.

(14) Xiong, B.; Zhao, P.; Hu, K.; Zhang, L.; Cheng, G. Dissolution of cellulose in aqueous NaOH/urea solution: role of urea. *Cellulose* **2014**, *21*, 1183−1192.

(15) Fu, F.; Yang, Q.; Zhou, J.; Hu, H.; Jia, B.; Zhang, L. Structure and properties of regenerated cellulose filaments prepared from cellulose carbamate−NaOH/ZnO aqueous solution. *ACS Sustainable Chem. Eng.* **2014**, *2*, 2604−2612.

(16) Fu, F.; Li, L.; Liu, L.; Cai, J.; Zhang, Y.; Zhou, J.; Zhang, L. Construction of cellulose based ZnO nanocomposite films with antibacterial properties through one-step coagulation. *ACS Appl. Mater. Interfaces* **2015**, *7*, 2597−2606.

(17) Li, R.; Zhang, L.; Xu, M. Novel regenerated cellulose films prepared by coagulating with water: Structure and properties. *Carbohydr. Polym.* **2012**, *87*, 95−100.

(18) Zhang, L.; Mao, Y.; Zhou, J.; Cai, J. Effects of coagulation conditions on the properties of regenerated cellulose films prepared in NaOH/Urea aqueous solution. *Ind. Eng. Chem. Res.* **2005**, *44*, 522−529.

(19) Huang, K.; Wang, Y. Recent applications of regenerated cellulose films and hydrogels in food packaging. *Curr. Opin. Food* **2022**, *43*, 7−17.

(20) Zhao, G.; Lyu, X.; Lee, J.; Cui, X.; Chen, W. N. Biodegradable and transparent cellulose film prepared eco-friendly from durian rind for packaging application. *Food Packag. Shelf Life* **2019**, *21*, No. 100345.

(21) Gu, R.; Yun, H.; Chen, L.; Wang, Q.; Huang, X. Regenerated cellulose films with amino-terminated hyperbranched polyamic anchored nanosilver for active food packaging. *ACS Appl. Bio Mater.* **2020**, *3*, 602−610.

(22) Ding, L.; Li, X.; Hu, L.; Zhang, Y.; Jiang, Y.; Mao, Z.; Xu, H.; Wang, B.; Feng, X.; Sui, X. A naked-eye detection polyvinyl alcohol/cellulose-based pH sensor for intelligent packaging. *Carbohydr. Polym.* **2020**, *233*, No. 115859.

(23) Chung, Y. C.; Lin, Y. Y.; Tseng, C. P. Control of H_2S waste gas emissions with a biological activated carbon filter. *J. Chem. Technol. Biotechnol.* **2004**, *79*, 570−577.

(24) Doujaiji, B.; Al-Tawfiq, J. A. Hydrogen sulfide exposure in an adult male. *Ann. Saudi Med.* **2010**, *30*, 76−80.

(25) Tabassum, R.; Mishra, S. K.; Gupta, B. D. Surface plasmon resonance-based fiber optic hydrogen sulphide gas sensor utilizing Cu−ZnO thin films. *Phys. Chem. Chem. Phys.* **2013**, *15*, 11868−11874.

(26) Ng, P. C.; Hendry-Hofer, T. B.; Witeof, A. E.; Brenner, M.; Mahon, S. B.; Boss, G. R.; Haouzi, P.; Bebarta, V. S. Hydrogen sulfide toxicity: Mechanism of action, clinical presentation, and countermeasure development. *J. Med. Toxicol.* **2019**, *15*, 287−294.

(27) Cheng, H.; Xu, H.; Julian McClements, D.; Chen, L.; Jiao, A.; Tian, Y.; Miao, M.; Jin, Z. Recent advances in intelligent food packaging materials: Principles, preparation and applications. *Food Chem.* **2022**, *375*, No. 131738.

(28) Caleb, O. J.; Mahajan, P. V.; Al-Said, F. A.; Opara, U. L. Modified Atmosphere Packaging Technology of Fresh and Fresh-cut Produce and the Microbial Consequences - a review. *Food Bioproc. Technol.* **2013**, *6*, 303−329.
(29) Koskela, J.; Sarfraz, J.; Ihalainen, P.; Määttänen, A.; Pulkkinen, P.; Tenhu, H.; Nieminen, T.; Kilpelä, A.; Peltonen, J. Monitoring the quality of raw poultry by detecting hydrogen sulfide with printed sensors. *Sens. Actuators, B* **2015**, *218*, 89−96.
(30) Kuswandi, B.; Wicaksono, Y.; Jayus; Abdullah, A.; Heng, L. Y.; Ahmad, M. Smart packaging: sensors for monitoring of food quality and safety. *Sens. Instrum. Food Qual. Saf.* **2011**, *5*, 137−146.
(31) Pandey, S. K.; Kim, K. H.; Tang, K.-T. A review of sensor-based methods for monitoring hydrogen sulfide. *TrAC, Trends Anal. Chem.* **2012**, *32*, 87−99.
(32) Ibrahim, H.; Serag, A.; Farag, M. A. Emerging analytical tools for the detection of the third gasotransmitter H_2S, a comprehensive review. *J. Adv. Res.* **2021**, *27*, 137−153.
(33) Pereira, P. F. M.; de Sousa Picciani, P. H.; Calado, V.; Tonon, R. V. Electrical gas sensors for meat freshness assessment and quality monitoring: a review. *Trends Food Sci. Technol.* **2021**, *118*, 36−44.
(34) Sanderson, H. P.; Thomas, R.; Katz, M. Limitations of the lead acetate impregnated paper tape method for hydrogen sulfide. *J. Air Pollut. Control. Assoc.* **1966**, *16*, 328−330.
(35) Chen, R.; Nuhfer, N. T.; Moussa, L.; Morris, H. R.; Whitmore, P. M. Silver sulfide nanoparticle assembly obtained by reacting an assembled silver nanoparticle template with hydrogen sulfide gas. *Nanotechnology* **2008**, *19*, 455604.
(36) Zhai, X.; Li, Z.; Shi, J.; Huang, X.; Sun, Z.; Zhang, D.; Zou, X.; Sun, Y.; Zhang, J.; Holmes, M.; Gong, Y.; Povey, M.; Wang, S. A colorimetric hydrogen sulfide sensor based on gellan gum-silver nanoparticles bionanocomposite for monitoring of meat spoilage in intelligent packaging. *Food Chem.* **2019**, *290*, 135−143.
(37) Jornet-Martínez, N.; Hakobyan, L.; Argente-García, A. I.; Molins-Legua, C.; Campíns-Falcó, P. Nylon-supported plasmonic assay based on the aggregation of silver nanoparticles: in situ determination of hydrogen sulfide-like compounds in breath samples as a proof of concept. *ACS Sens.* **2019**, *4*, 2164−2172.
(38) Pla-Tolós, J.; Moliner-Martínez, Y.; Verdú-Andrés, J.; Casanova-Chafer, J.; Molins-Legua, C.; Campíns-Falcó, P. New optical paper sensor for in situ measurement of hydrogen sulphide in waters and atmospheres. *Talanta* **2016**, *156-157*, 79−86.
(39) Engel, L.; Benito-Altamirano, I.; Tarantik, K. R.; Pannek, C.; Dold, M.; Prades, J. D.; Wöllenstein, J. Printed sensor labels for colorimetric detection of ammonia, formaldehyde and hydrogen sulfide from the ambient air. *Sens. Actuators B Chem.* **2021**, *330*, No. 129281.
(40) Phuangsaijai, N.; Jakmunee, J.; Kittiwachana, S. Investigation into the predictive performance of colorimetric sensor strips using RGB, CMYK, HSV, and CIELAB coupled with various data preprocessing methods: a case study on an analysis of water quality parameters. *J. Anal. Sci. Technol.* **2021**, *12*, 19.
(41) Leal, V. G.; Batista, A. D.; Petruci, J. F. D. S. 3D-printed and fully portable fluorescent-based platform for sulfide determination in waters combining vapor generation extraction and digital images treatment. *Talanta* **2021**, *222*, No. 121558.
(42) Engel, L.; Tarantik, K. R.; Pannek, C.; Wöllenstein, J. Screen-printed sensors for colorimetric detection of hydrogen sulfide in ambient air. *Sensors* **2019**, *19*, 1182.
(43) Carpenter, T. S.; Rosolina, S. M.; Xue, Z. L. Quantitative, colorimetric paper probe for hydrogen sulfide gas. *Sens. Actuators, B* **2017**, *253*, 846−851.
(44) Gong, J.; Li, J.; Xu, J.; Xiang, Z.; Mo, L. Research on cellulose nanocrystals produced from cellulose sources with various polymorphs. *RSC Adv.* **2017**, *7*, 33486−33493.
(45) Wei, Q. Y.; Lin, H.; Yang, B.; Li, L.; Zhang, L. Q.; Huang, H. D.; Zhong, G. J.; Xu, L.; Li, Z. M. Structure and properties of all-cellulose composites prepared by controlling the dissolution temperature of a NaOH/Urea solvent. *Ind. Eng. Chem. Res.* **2020**, *59*, 10428−10435.
(46) Fouad, H.; Kian, L. K.; Jawaid, M.; Alotaibi, M. D.; Alothman, O. Y.; Hashem, M. Characterization of microcrystalline cellulose isolated from conocarpus fiber. *Polymer* **2020**, *12*, 2926.
(47) Pang, J. H.; Liu, X.; Wu, M.; Wu, Y. Y.; Zhang, X. M.; Sun, R. C. Fabrication and characterization of regenerated cellulose films using different ionic liquids. *J. Spectrosc.* **2014**, *2014*, 214057.
(48) Zheng, W.; Yang, Z.; Yang, J.; Qu, W.; Feng, Y.; Jiang, S.; Zhao, S.; Shih, K.; Li, H. Favorably adjusting the pore characteristics of copper sulfide by template regulation for vapor-phase elemental mercury immobilization. *J. Mater. Chem. A* **2022**, *10*, 10729−10737.
(49) Wang, Z.; Liu, J.; Zhang, L.; Nie, W.; Liu, J.; Yang, J.; Li, Y. Copper (II)-azo complex modified hydrogel: a sensitive colorimetric sensor for visual detection of H_2S gas. *Sens. Actuators, B* **2023**, *376*, No. 132968.
(50) Mamaeva, A. A.; Martynov, V. I.; Deyev, S. M.; Pakhomov, A. A. Comparison of colorimetric and fluorometric chemosensors for protein concentration determination and approaches for estimation of their limits of detection. *Chemosensors* **2022**, *10*, 542.
(51) Jarosz, A. P.; Yep, T.; Mutus, B. Microplate-based colorimetric detection of free hydrogen sulfide. *Anal. Chem.* **2013**, *85*, 3638−3643.
(52) Das, S.; Sahoo, P. A colorimetric sensor for hydrogen sulfide: Detection from biogas and quantitative estimation in water. *Sens. Actuators, B* **2019**, *291*, 287−292.
(53) Zhang, Z.; Chen, Z.; Wang, S.; Qu, C.; Chen, L. On-site visual detection of hydrogen sulfide in air based on enhancing the stability of gold nanoparticles. *ACS Appl. Mater. Interfaces* **2014**, *6*, 6300−6307.
(54) Yuan, Z.; Lu, F.; Peng, M.; Wang, C.-W.; Tseng, Y.-T.; Du, Y.; Cai, N.; Lien, C. W.; Chang, H. T.; He, Y.; Yeung, E. S. Selective colorimetric detection of hydrogen sulfide based on primary amine-active ester cross-linking of gold nanoparticles. *Anal. Chem.* **2015**, *87*, 7267−7273.

https://doi.org/10.1021/acsomega.3c01449
ACS Omega 2023, 8, 17134−17142